Supplement of Atmos. Chem. Phys., 24, 10759–10772, 2024
https://doi.org/10.5194/acp-24-10759-2024-supplement

Atmospheric Chemistry and Physics
Open Access
EGU

Supplement of

Assessing the effectiveness of SO_2, NO_x, and NH_3 emission reductions in mitigating winter $PM_{2.5}$ in Taiwan using CMAQ

Ping-Chieh Huang et al.

Correspondence to: Hui-Ming Hung (hmhung@ntu.edu.tw)

Contents of this file

Relationship between S_{NOx,NO_3} and NO_2 concentration

The reduction in NOx emissions leads to a decrease in NO_2 concentration, subsequently reducing HNO_3 production through reaction R1:

$$NO_2 + OH \rightarrow HNO_3 \quad (R1)$$

The production rate of HNO_3 (P_{HNO3}) can be calculated by assuming that OH concentration is in the steady state as follows:

$$\frac{d[OH]}{dt} = P_r - L = P - \sum k_i[A]_i\,[OH] - k_{NO_2}[NO_2][OH], \quad (1)$$

where P_r and L are chemical production and loss of [OH], respectively, $\sum k_i[A]_i\,[OH]$ is the sum of reaction rates of all OH-consuming chemical reactions except reaction (R1), k_i is the rate constant of each reaction.

The steady-state [OH] is estimated as follows:

$$[OH]_{SS} = \frac{P_r}{\sum k_i[A]_i + k_{NO_2}[NO_2]} \quad (2)$$

Thus, the production rate of HNO_3 is:

$$P_{HNO_3} = k_{NO_2}[NO_2][OH]_{SS} = \frac{P_r \times k_{NO_2}[NO_2]}{\sum k_i[A]_i + k_{NO_2}[NO_2]} \quad (3)$$

The total [HNO_3] is contributed by the chemical process ($[HNO_3]_{chem}$) at a time frame of Δt and transported from outside the domain boundaries ($[HNO_3]_{trans}$) as follows:

$$[HNO_3] = [HNO_3]_{chem} + [HNO_3]_{trans} = \frac{P_r \times k_{NO_2}[NO_2]\Delta t}{\sum k_i[A]_i + k_{NO_2}[NO_2]} + [HNO_3]_{trans} \quad (4)$$

When [NO_2] is sufficiently low, $[HNO_3]_{trans}$ becomes comparable with $[HNO_3]_{chem}$ to affect the total [HNO_3]. Assuming [NO_2] is proportional to the emission ratio (*Er*), we have [NO_2] = $[NO_2]_{control\_run} \times Er$,. With the assumptions of $P_r \times \Delta t = 3$ and $\sum k_i[A]_i : k_{NO_2}[NO_2]_{control\_run} = 7 : 5$, the influence of transport term on the sensitivity, S_{NOx,NO_3} can be evaluated. Figure S14 shows HNO_3 concentration and S_{NOx,NO_3} under conditions with $[HNO_3]_{trans}$ = 0, 0.2, and 0.53, representing no transported HNO_3, transported HNO_3 equal to $[HNO_3]_{chem}$ at NO_2 = 0.1 and at NO_2 = 0.3, respectively. HNO_3 increases as *Er* increases, but the increase gradually slows down. Variations in transported HNO_3 do not alter the overall pattern of total HNO_3 but do introduce differences in values (Fig. S14a). However, the trend of S_{NOx,NO_3} is different (Fig. S14b). Without transported HNO_3, S_{NOx,NO_3} increases as *Er* decreases. Conversely, when $[HNO_3]_{trans}$ is greater than 0, S_{NOx,NO_3} shows a transition point occurring at *Er*, corresponding to $[HNO_3]_{chem}$ similar to $[HNO_3]_{trans}$. The scatter plot of S_{NOx,NO_3}, calculated from six

discrete points with an interval of 0.2 to mimic the CMAQ simulation, shows a similar trend under the influence of non-zero $[HNO_3]_{trans}$.

Table S1: WRF-CMAQ model setting.

	Parameters	Setting
WRF v3.7.1	Microphysics	WSM 5-class scheme
	Cumulus Parameterization	Kain-Fritsch
	Planetary Boundary Layer	YSU scheme
	Surface Layer	MM5 Monin-Obukhov scheme
	Land Surface	Unified Noah land-surface model
	Urban Surface	No
	Longwave Radiation	cam scheme
	Shortwave Radiation	cam scheme
	SST_update	Yes
CMAQ v5.2.1	Chemical mechanism	Cb06
	Horizontal advection	Yamo
	Vertical advection	WRF input
	Horizontal mixing/diffusion	Multiscale
	Aerosol	Aero 6
	Cloud option	ACM AE6
	Emission	TEDS 9.0

Table S2: WRF-CMAQ resolution.

		D01	D02	D03	D04
WRF	**Vertical Layer**	45	45	45	45
	Grid size	91×91	166×169	223×223	223×223
	FDDA	Yes	Yes	Yes	No
CMAQ	**Resolution**	81km	27km	9km	3km
	Vertical Layer	6	15	15	15
	Grid size	70×80	70×80	70×80	90×135

Table S3: Box model initial conditions.

parameter	value	Description*
Temperature	291 K	
Cloud water	0.376 g kg^{-1}	
$CO_{2(g)}$	400 ppmv	Constant
$SO_{2(g)}$	7.13 ppbv	[b]$SO_{2(g)}$ + [c]dH_2O_2
[a]$H_2O_{2(g)}$	0.43 ppbv	
[b]$O_{3(g)}$	18.7 ppbv	
Total [a]NH_3	73.4 ppbv × [d]*Er*	$NH_{3(g)}$ + NH_4^+(I+J+K)
Total [a]HNO_3	12.3 ppbv	$HNO_{3(g)}$ + NO_3^-(I+J+K)
SO_4^{2-}	0.088 μg m^{-3}	[b]SO_4^{2-}(I+J+K) – [c]dH_2O_2
[a]Fe^{3+}	0.0238 μg m^{-3}	Fe(III) available for sulfate oxidation
[a]Mn^{2+}	0.035 μg m^{-3}	Mn(II) available for sulfate oxidation
[a]Na^+	0.48	I+J+K
[a]K^+	0.82	J+K
[a]Ca^{2+}	1.38	J+K
[a]Mg^{2+}	1.00	J+K
[a]Cl^-	0.64	I+J+K

* I, J, K denotes Aitken, accumulation, and coarse modes in particle phase from CMAQ output.

* Condition: a grid point along the coast of Taichung (24.203° N, 120.5053° E, the second layer, ~ 68.5 m a.s.l) at 8:00 am local time on 3rd December 2018 from CMAQ.

[a] The concentration from the control run.

[b] The concentration from the NH3_02x run (NH_3 emission reduced to 0.2x of control run).

[c] dH_2O_2 is the H_2O_2 difference concentration (control run – NH3-02x run).

[d] *Er* ranges from 0.2 to 1.0 at 0.1 intervals

Table S4: Reactions and rate constants used in the box model (from Seinfeld and Pandis (2006))

Dissolution reaction		**Henry's constant (M atm^{-1})**
1.	$CO_2 + H_2O \leftrightarrow CO_2 \cdot H_2O$	$H_{CO_2} = 0.034$
2.	$SO_2 + H_2O \leftrightarrow SO_2 \cdot H_2O$	$H_{SO_2} = 1.23$
3.	$HNO_{3(g)} \leftrightarrow HNO_{3(aq)}$	$H_{HNO_3} = 2.1 \times 10^5$
4.	$NH_3 + H_2O \leftrightarrow NH_3 \cdot H_2O$	$H_{NH_3} = 62$
5.	$O_{3(g)} \leftrightarrow O_{3(aq)}$	$H_{O_3} = 1.14 \times 10^{-2}$
6.	$H_2O_{2(g)} \leftrightarrow H_2O_{2(aq)}$	$H_{H_2O_2} = 1 \times 10^5$
Dissociation reaction		**Rate constant (M)**
7.	$CO_2 \cdot H_2O \leftrightarrow HCO_3^- + H^+$ $HCO_3^- \leftrightarrow CO_3^{2-} + H^+$	$k_{c1} = 4.2 \times 10^{-7}$ $k_{c2} = 5.61 \times 10^{-11}$
8.	$SO_2 \cdot H_2O \leftrightarrow HSO_3^- + H^+$ $HSO_3^- \leftrightarrow SO_3^{2-} + H^+$	$k_{s1} = 1.3 \times 10^{-2}$ $k_{s2} = 6.6 \times 10^{-8}$
9.	$HNO_{3(aq)} \leftrightarrow NO_3^- + H^+$	$k_{a1} = 15.4$
10.	$NH_3 \cdot H_2O \leftrightarrow NH_4^+ + OH^-$	$k_{a1} = 1.7 \times 10^{-5}$
11.	$H_2SO4 \leftrightarrow HSO_4^- + H^+$ $HSO_4^- \leftrightarrow SO_4^{2-} + H^+$	as a complete dissociation $k_{a2} = 1.2 \times 10^{-2}$
12.	$H_2O \leftrightarrow H^+ + OH^-$	
Aqueous oxidation reaction		**Rate constant (M^{-1}s^{-1})**
13.	$SO_2 + O_3 + H_2O \rightarrow SO_4^{2-} + O_2 + 2H^+$ $HSO_3^- + O_3 \rightarrow SO_4^{2-} + O_2 + H^+$ $SO_3^{2-} + O_3 \rightarrow SO_4^{2-} + O_2$	$k_{O_3,1} = 2.4 \times 10^4$ $k_{O_3,2} = 3.7 \times 10^5$ $k_{O_3,2} = 1.5 \times 10^9$
14.	$HSO_3^- + H_2O_2 + H^+ \rightarrow SO_4^{2-} + 2H^+ + H_2O$	$k_{H_2O_2} = 7.45 \times 10^7$
15.	$S(IV) + \frac{1}{2}O_2 \xrightarrow{Mn^{2+},Fe^{3+}} S(VI)$	$k_{Mn} = 750; k_{Fe} = 2600;$ $k_{Mn,Fe} = 1.0 \times 10^{10}$

Table S5: Statistics of air temperature, relative humidity, CO, and O_3 of MOENV observation and model simulation results.

	Tamsui	Shalu	Taixi	Qianzhen
Temperature (degree C)				
Mean value of MOENV	18.61	20.19	20.00	23.31
Mean value of WRF	18.48	19.50	19.05	22.39
Correlation coefficient	0.87	0.93	0.84	0.93
Mean bias error	-0.18	-0.69	-0.95	-0.92
Mean absolute error	1.33	1.10	1.47	1.34
RH (%)				
Mean value of MOENV	85.12	74.97	82.85	69.49
Mean value of WRF	80.42	76.49	80.71	69.95
Correlation coefficient	0.71	0.84	0.58	0.86
Mean bias error	-4.23	1.52	-2.14	0.46
Mean absolute error	7.31	6.23	6.75	4.78
CO (ppbv)				
Mean value of MOENV	331.98	355.42	258.98	644.20
Mean value of CMAQ	137.84	143.09	129.03	266.13
Correlation coefficient	0.59	0.53	0.46	0.62
Mean bias error	-194.05	-212.32	-129.94	-377.72
Mean absolute error	196.13	212.32	130.95	378.77
O_3 (ppbv)				
Mean value of MOENV	35.05	31.43	37.74	26.77
Mean value of CMAQ	47.13	42.73	42.57	32.51
Correlation coefficient	0.66	0.73	0.58	0.84
Mean bias error	12.07	11.29	4.67	5.76
Mean absolute error	13.0	12.93	8.94	11.05

$$\text{Correlation coefficient} = \frac{\sum_{i=1}^{n}(m_i-\bar{m})(o_i-\bar{o})}{\sqrt{\sum_{i=1}^{n}(m_i-\bar{m})^2}\sqrt{\sum_{i=1}^{n}(o_i-\bar{o})^2}}$$

$$\text{Mean bias error} = \overline{(m_\iota - o_\iota)};\ \text{Mean absolute error} = \overline{|(m_\iota - o_\iota)|}$$

where m_i and o_i are the wind speed or concentrations of model and observation at time i, respectively, and $\bar{m}$ and $\bar{o}$ are their average over December 2018.

Table S6: Mean contribution of sulfate formation in each air pollution zone (elevation below 200 m a.s.l.).

	Gas phase processes	Aqueous phase processes	Other processes
northern Taiwan	8.4%	21.5%	70.1%
Chu-Miao area	11.2%	28.5%	60.3%
central Taiwan	13.2%	30.5%	56.3%
Yun-Chia-Nan area	16.5%	27.6%	55.9%
Kao-Ping area	19.8%	23.7%	56.6%

Table S7: Statistics of the sensitivity of emission reductions on $PM_{2.5}$ concentration for NOx ($S_{NOx,PM_{2.5}}$) and NH_3 ($S_{NH_3,PM_{2.5}}$) in each air pollution zone (elevation below 200 m a.s.l.) under current conditions (at NOx emission ratio of 0.9).

	$S_{NOx,PM_{2.5}}$			$S_{NH_3,PM_{2.5}}$		
	Mean	**Q1**	**Q3**	**Mean**	**Q1**	**Q3**
Northern Taiwan	0.15	0.12	0.19	0.12	0.11	0.14
Chu-Miao area	0.20	0.18	0.22	0.17	0.16	0.19
Central Taiwan	0.23	0.20	0.25	0.19	0.18	0.21
Yun-Chia-Nan area	0.33	0.30	0.36	0.19	0.18	0.20
Kao-Ping area	0.34	0.31	0.41	0.19	0.17	0.21

Mean: arithmetic mean; Q1: 25th percentile; Q3: 75th percentile.

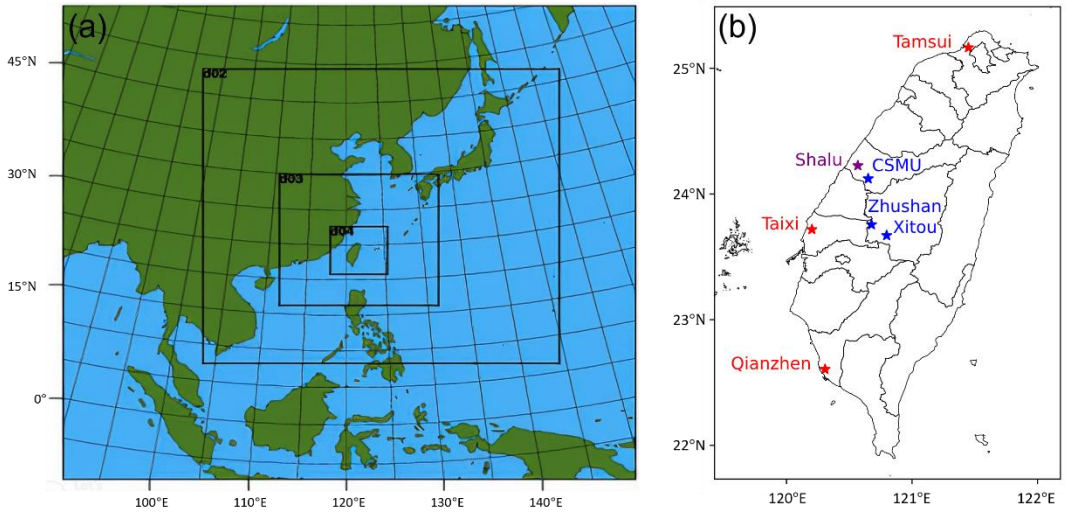

Figure S1: (a) WPS domain configuration. (b) CMAQ d04 domain. Red points (★) are MOENV stations, blue points (★) indicate PM components measurement stations, and purple point (★) is Shalu station, having both MOENV data and PM components data.

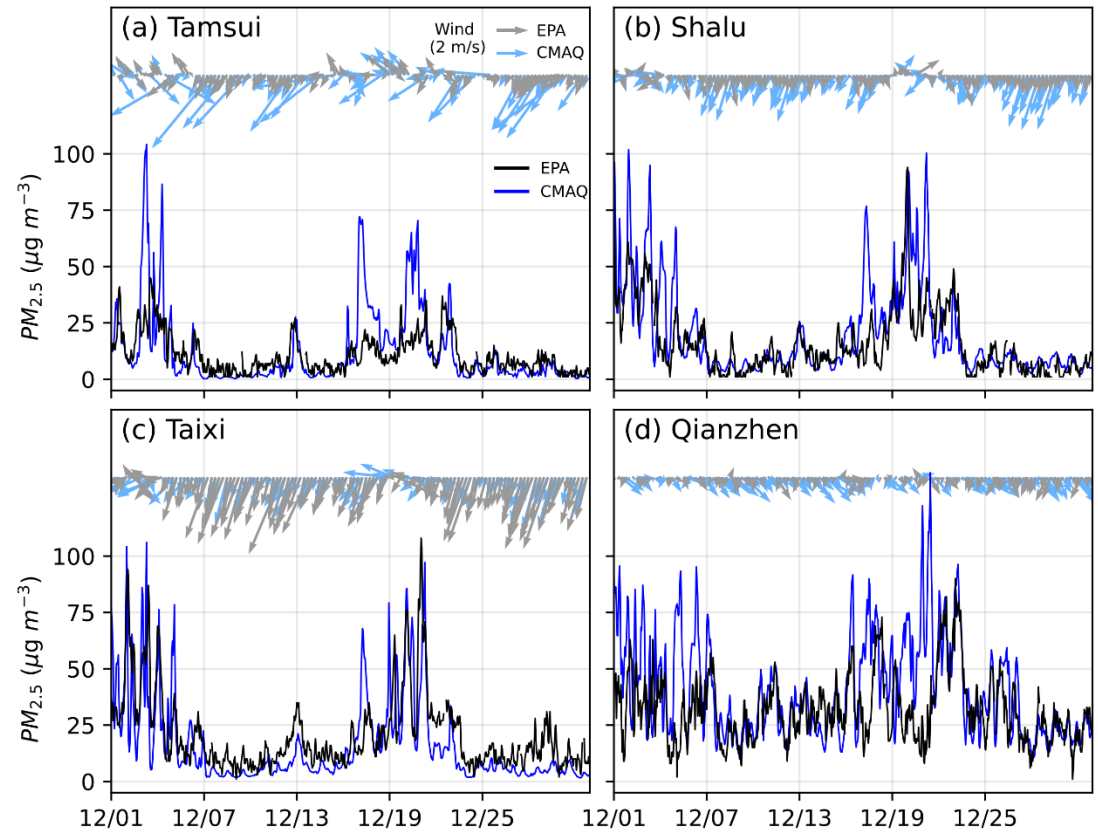

Figure S2: The comparison of wind field and $PM_{2.5}$ between MOENV ground observations and CMAQ surface layer data.

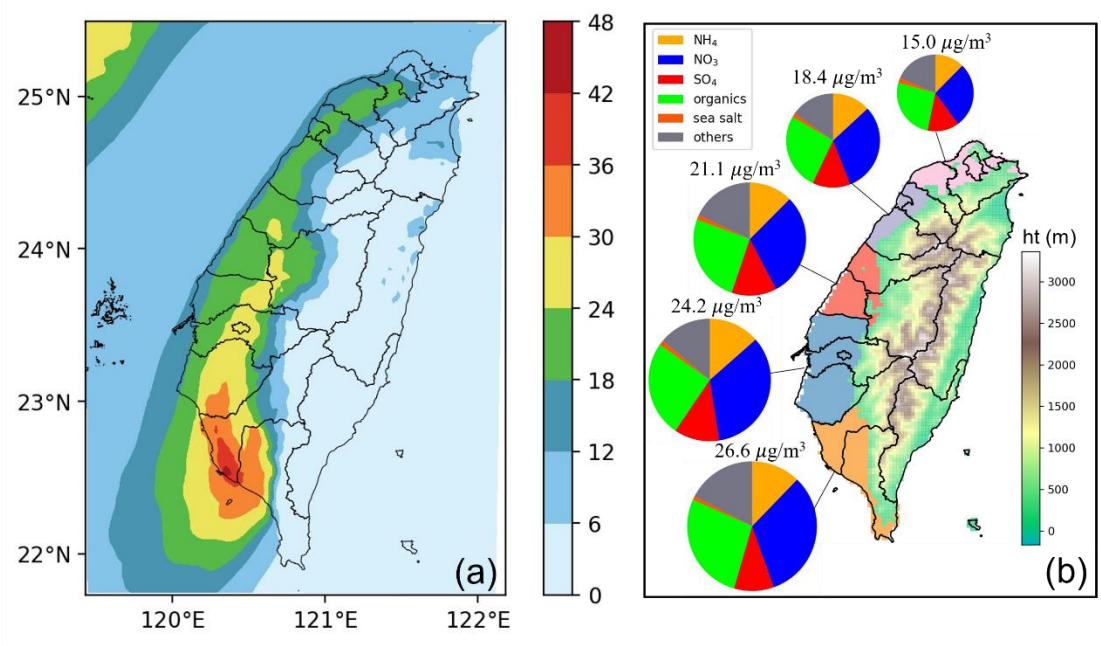

Figure S3: Model results for (a) Average $PM_{2.5}$ concentration (μg m^{-3}). (b) The composition fraction and $PM_{2.5}$ concentrations for different regions (different shading colors) for elevation less than 200 m a.s.l. (the regions from north to south are northern Taiwan (pink), Chu-Miao (purple), central Taiwan (red), Yun-Chia-Nan (blue), and Kao-Ping (orange)). The components are shown in legend. The color bar is the height above sea level. Conditions: average data for December 2018 at the surface layer.

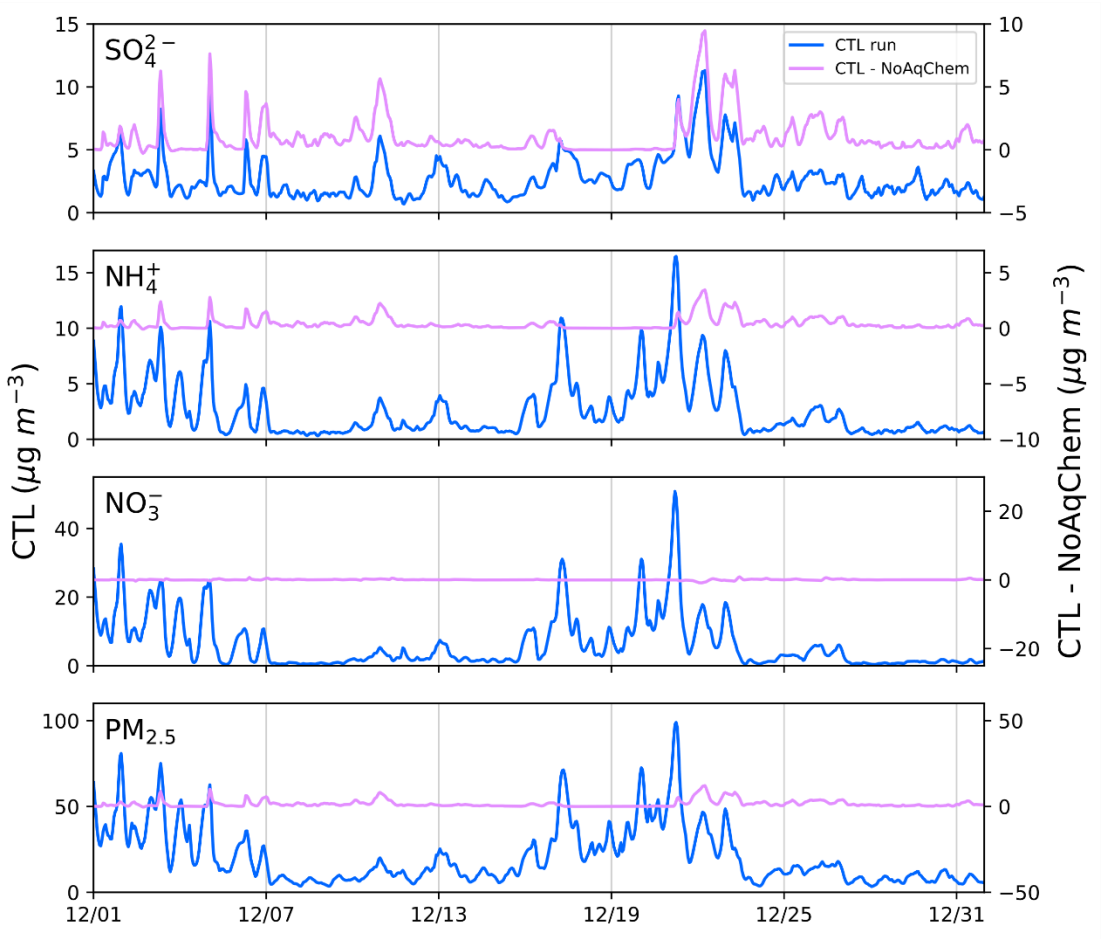

Figure S4: Sulfate, ammonium, nitrate, and $PM_{2.5}$ concentrations of control run (blue line, left y-axis) and the difference between control and NoAqChem runs (pink line, right y-axis). The left and right y-axes have the same scale but different ranges. Conditions: average data for central Taiwan at the surface layer.

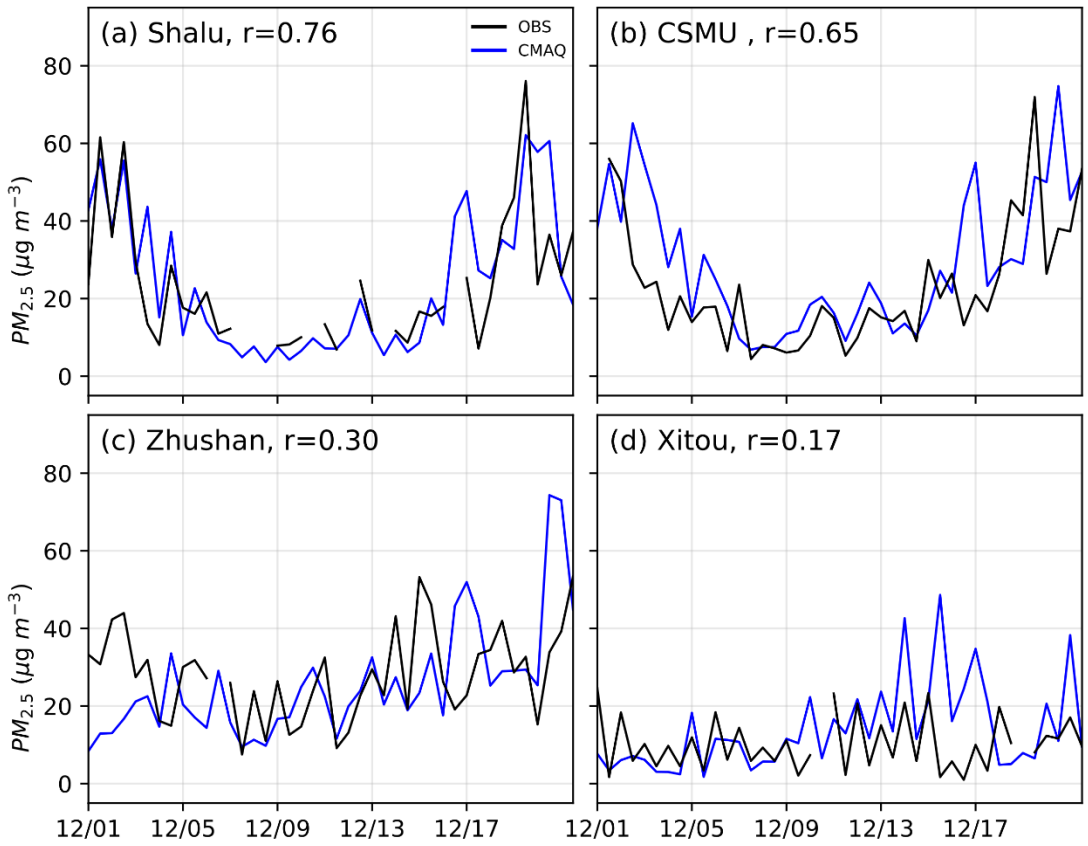

Figure S5: The comparison of $PM_{2.5}$ between observation and CMAQ surface layer data in central Taiwan (r: correlation coefficient).

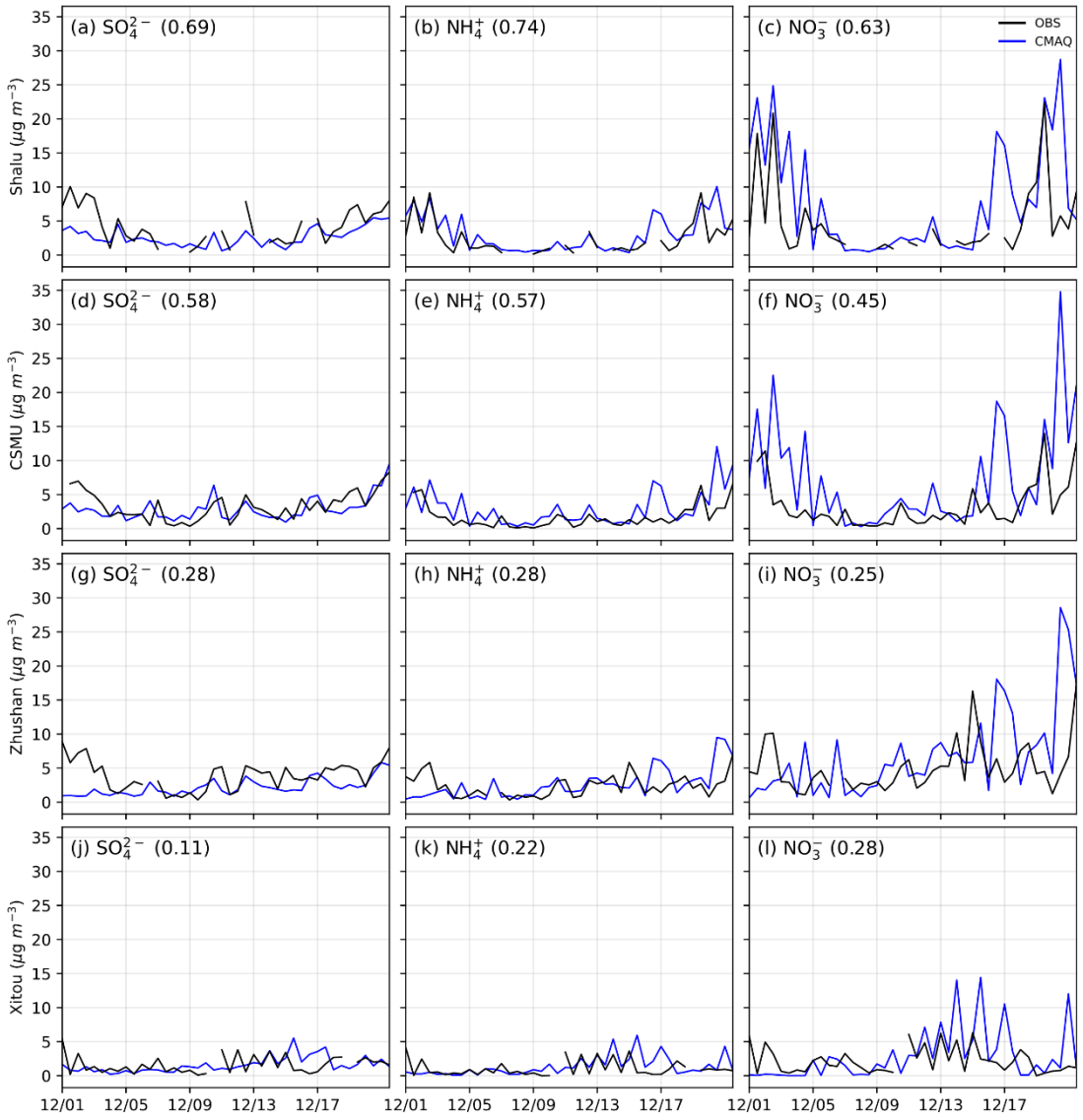

Figure S6: The comparison of sulfate, ammonium, and nitrate between observation and CMAQ surface layer data in central Taiwan (the correlation coefficients indicated in parentheses).

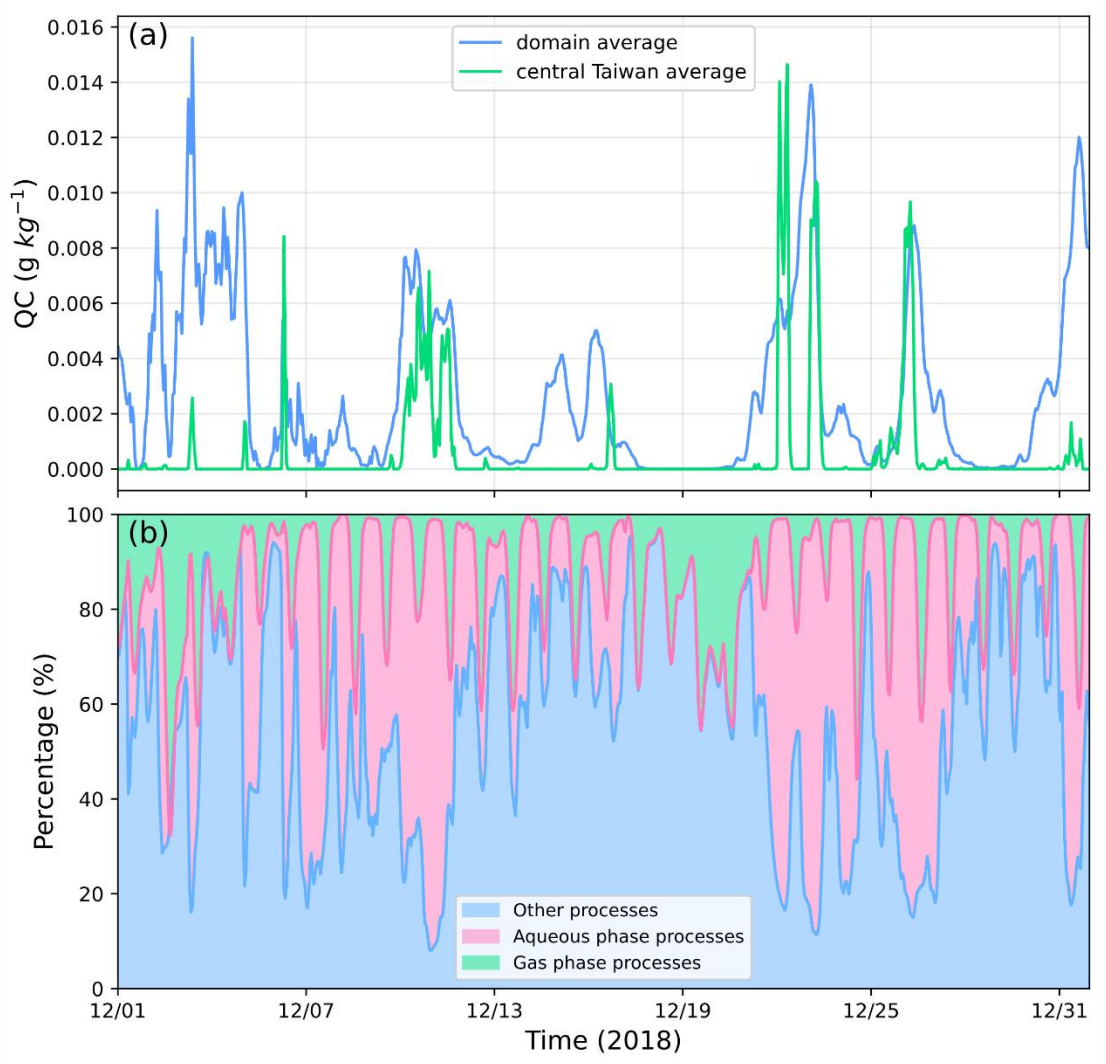

Figure S7: (a) Average cloud water content within the planetary boundary layer. (b) Surface layer average sulfate source contributions in central Taiwan.

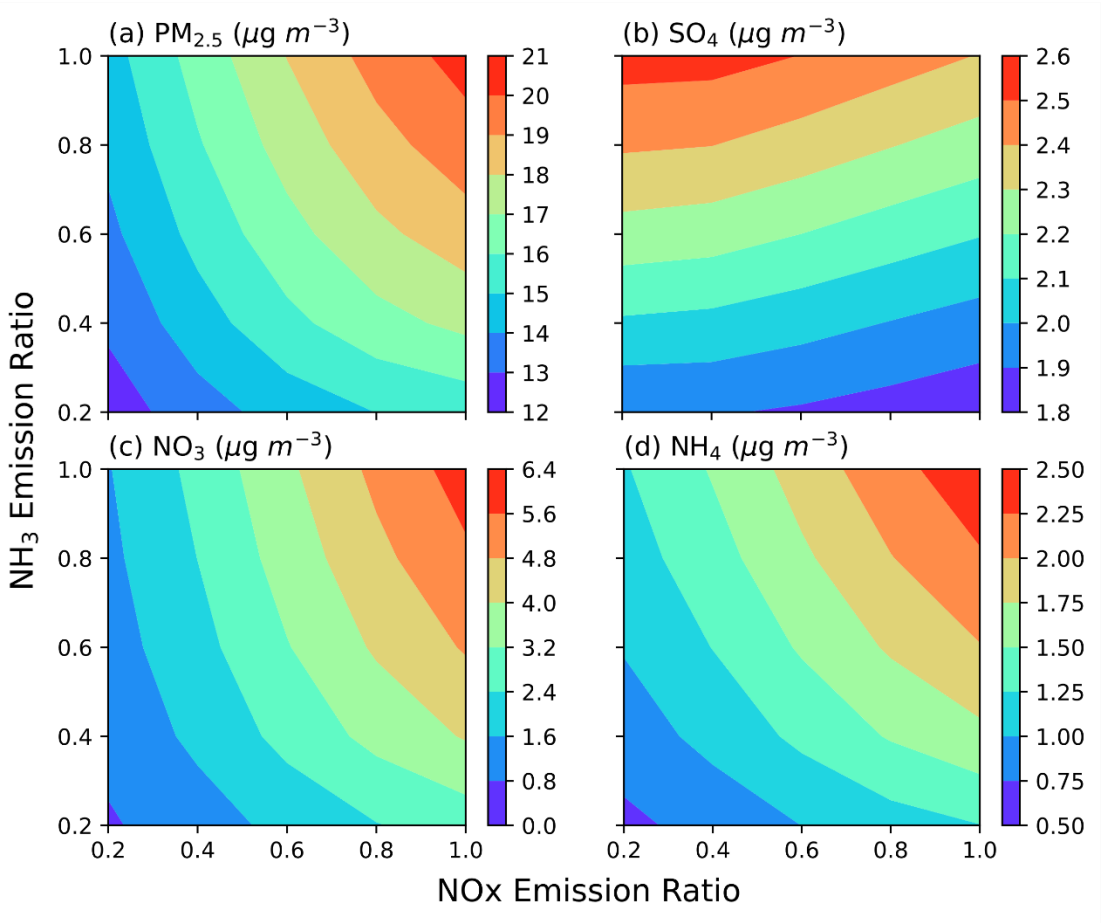

Figure S8: (a) $PM_{2.5}$, (b) sulfate, (c) nitrate, and (d) ammonium average concentrations as a function of NOx (x-axis) and NH_3 (y-axis) emission ratios. Conditions: average data of central Taiwan from 1st to 14th December 2018 at the surface layer.

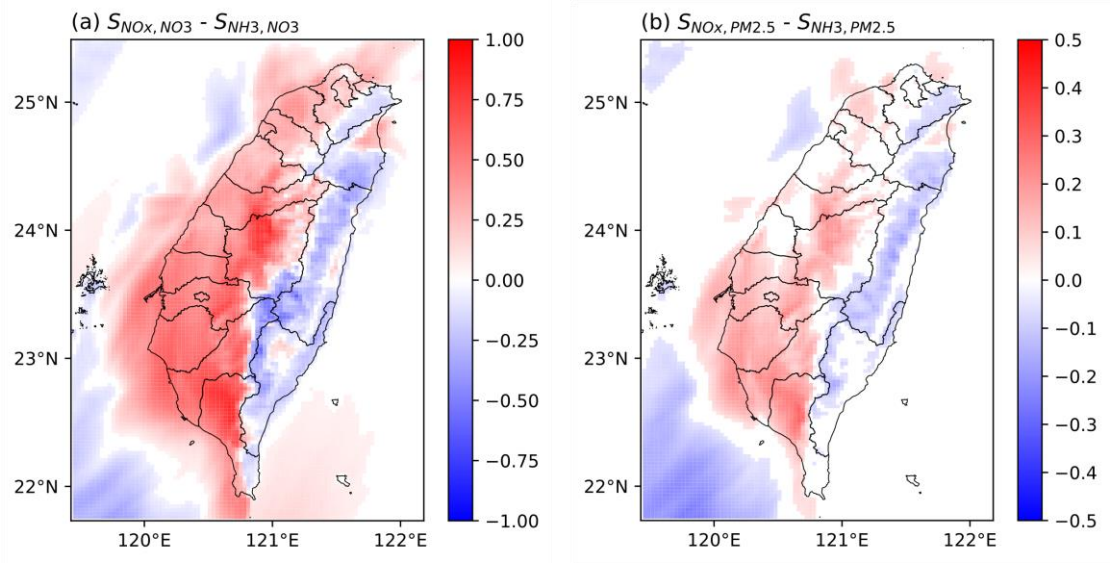

Figure S9: The difference in sensitivity map of (a) nitrate and (b) $PM_{2.5}$ between NOx and NH_3 under the current condition (at NOx emission ratio of 0.9). Red areas (positive) represent NOx-sensitive, blue areas (negative) represent NH_3-sensitive, and white areas represent neutral with values between -0.05 and 0.05. Conditions: average data for December 2018 at the surface layer.

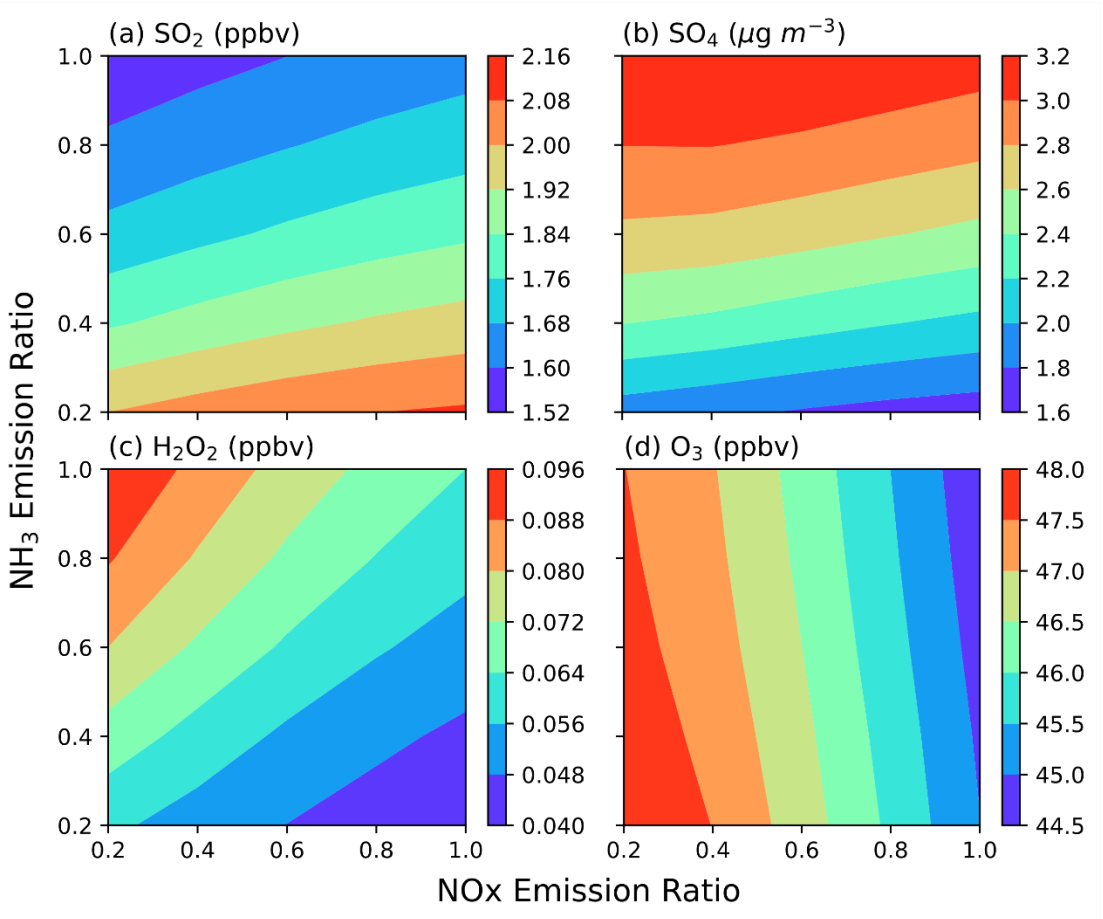

Figure S10: Average in-cloud concentrations of (a) SO_2, (b) sulfate, (c) H_2O_2, and (d) O_3 as a function of NOx (x-axis) and NH_3 (y-axis) emission ratios. Conditions: average data for the cloud grid points of western Taiwan land regions in domain 4 from 1st to 14th December 2018.

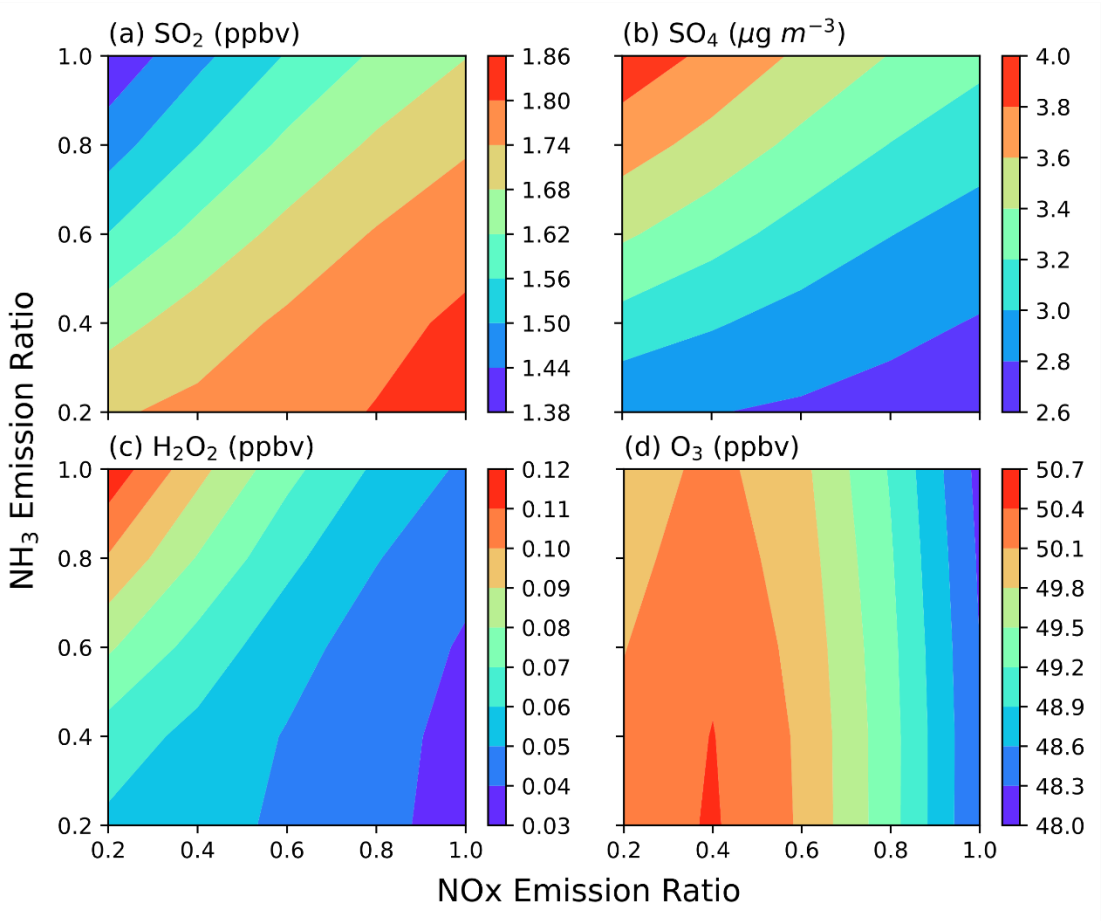

Figure S11: Average in-cloud concentrations of (a) SO_2, (b) sulfate, (c) H_2O_2, and (d) ozone as a function of NOx (x-axis) and NH_3 (y-axis) emission ratios. Conditions: average data for the cloud grid points of sea regions, west of 121°E in domain 4, from 1st to 14th December 2018.

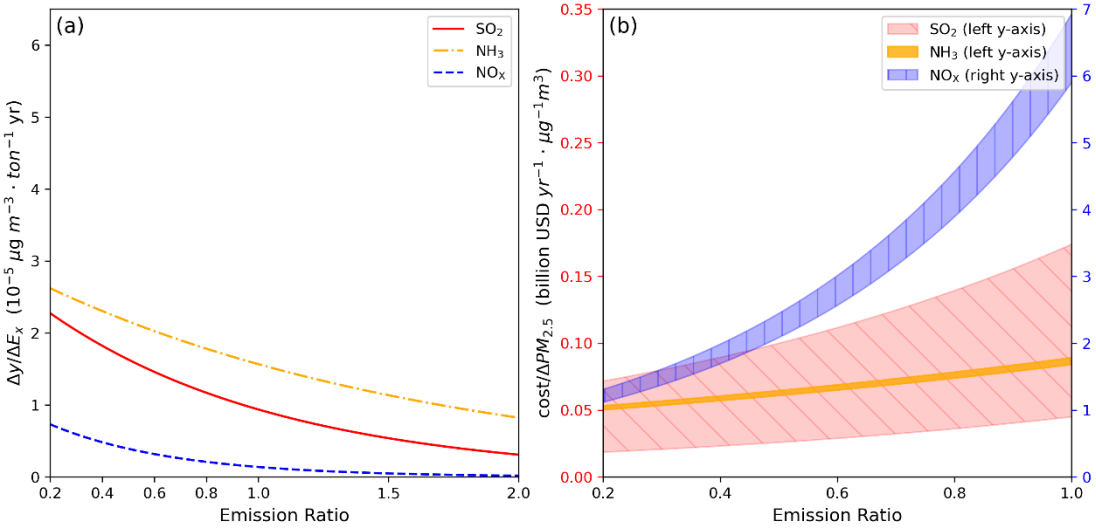

Figure S12: (a) $PM_{2.5}$ reduction efficiency and (b) reduction cost as a function of emission ratio for SO_2, NH_3, and NOx during the clean period of 6th-12th December 2018.

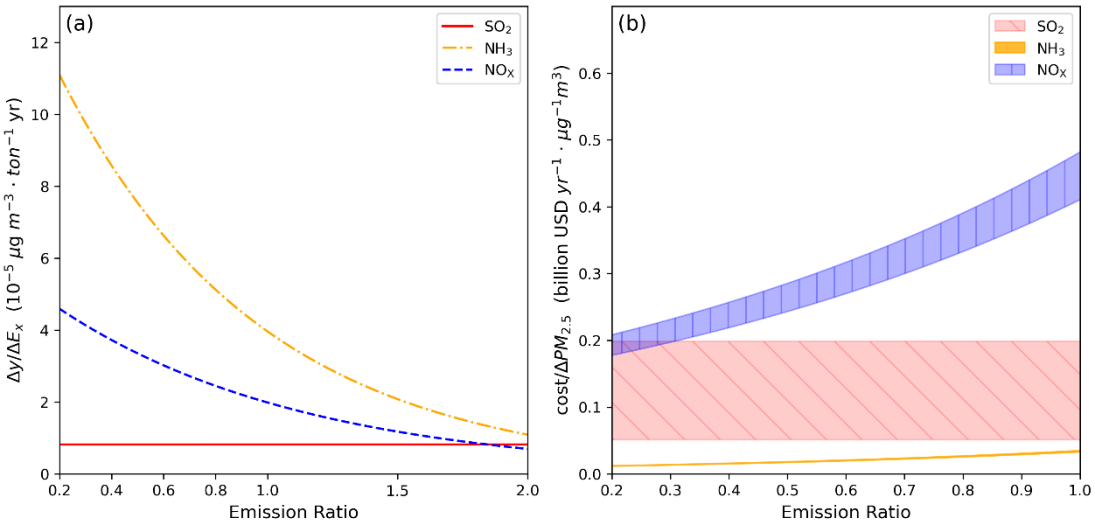

Figure S13: (a) $PM_{2.5}$ reduction efficiency and (b) reduction cost as a function of emission ratio for SO_2, NH_3, and NOx during the high pollution period of 16th-22th December 2018.

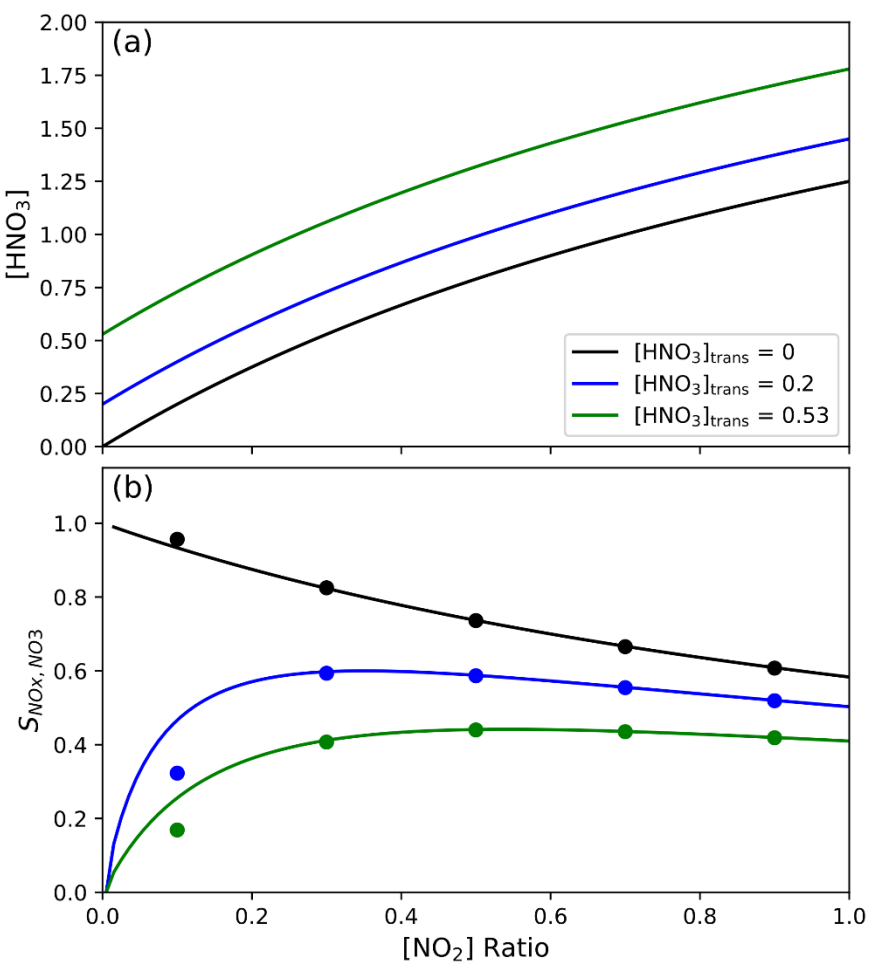

Figure S14: (a) HNO_3 concentration and (b) nitrate sensitivity coefficient of NOx (S_{NOx,NO_3}) as a function of NO_2 emission ratio for three conditions of $[HNO_3]_{trans}$ = 0, 0.2, and 0.53.

Reference

Seinfeld, J. H., and Pandis, S. N.: Atmospheric Chemistry and Physics: From Air Pollution to Climate Change, Wiley, 2006.